The Research of Medical Science Review
ISSN: 3007-1208 & 3007-1216 Volume 3, Issue 11, 2025

ENHANCED TISSUE REGENERATION USING BIOACTIVE HYDROGEL COMPOSITES REINFORCED WITH ZINC OXIDE NANOPARTICLES

Asia Noureen[1], Sara Khan Sherani[2], Samiyah Tasleem[3], Afroz Rais[4], Wali Muhammad Achakzai[5], Uzma Khan[6], Sonia Tabasum[*7]

[1]*Center for Interdisciplinary research in basic Sciences (CIRBS) International Islamic university Islamabad Pakistan*
[2]*Bachelor of Dental Surgery, Khyber College of Dentistry, Peshawar*
[3]*Department of Applied Science, Faculty of Engineering Science & Technology Hamdard University Karachi.*
[4]*Department of Botany, Sardar Bahadur Khan Women's University, Quetta*
[5]*Department of Zoology, University of Baluchistan Quetta*
[6]*Institute of Microbiology and Biotechnology, Bacha Khan University Charsadda*
[*7]*Department of Biochemistry, University of Agriculture Faisalabad*

[*7]sonialiaqat275@gmail.com

DOI: https://doi.org/10.5281/zenodo.17759095

Keywords
Zinc oxide nanoparticles; Bioactive hydrogels; Wound healing; Tissue regeneration; Antimicrobial biomaterials

Article History
Received: 06 October 2025
Accepted: 14 November 2025
Published: 29 November 2025

Corresponding Author: *
Sonia Tabasum

Abstract

Hydrogel-based biomaterials are widely used in tissue regeneration, yet their clinical performance is limited by weak mechanical strength, rapid degradation, and insufficient biological bioactivity. This study evaluates bioactive hydrogel composites reinforced with zinc oxide nanoparticles (ZnO-NPs) at concentrations of 1%, 2%, and 3% to improve mechanical stability, antimicrobial activity, and regenerative capacity. Mechanical analysis showed that ZnO-NP incorporation increased compressive modulus from 9.8 ± 1.2 kPa in the control to 41.7 ± 2.8 kPa, reflecting a 325% improvement, while compressive strength increased from 32.5 ± 3.7 kPa to 67.2 ± 4.5 kPa. Swelling behavior decreased from 410 ± 18% to 301 ± 12%, and degradation rate reduced from 58.3 ± 3.4% to 24.8 ± 2.1% over 14 days. Sustained Zn^{2+} release was observed, rising from 0.62 ± 0.05 ppm to 3.94 ± 0.21 ppm across the study period. Biological assays revealed enhanced fibroblast proliferation, increasing from baseline 100% viability to 159 ± 8% at 72 hours in 3% ZnO-NP hydrogels. Antimicrobial testing demonstrated strong inhibition against E. coli (up to 18.2 ± 1.1 mm) and S. aureus (up to 17.5 ± 1.2 mm). In vivo wound-healing analysis confirmed accelerated tissue repair, with wound closure reaching 92.4 ± 3.1% by day 14 compared to 74.2 ± 4.5% in hydrogel-only and 58.6 ± 5.3% in untreated controls. Histologically, ZnO-treated wounds showed a 182 ± 12 μm epithelial layer, 71.5 ± 4.1% collagen density, and 24.6 ± 2.3 microvessels per field. Overall, ZnO-NP hydrogels significantly enhance mechanical, antimicrobial, and regenerative performance, making them strong candidates for advanced wound-healing applications.

INTRODUCTION

Tissue regeneration continues to be a major focus within regenerative medicine, where engineered biomaterials are designed to restore or enhance the functional properties of damaged tissues[1]. Hydrogels have emerged as one of the most versatile scaffolding materials due to their high water content (typically 70–95%), excellent biocompatibility, and structural resemblance to the natural extracellular matrix (ECM)[2]. Their hydrated, porous architecture facilitates nutrient transport, supports cellular infiltration, and allows for incorporation of biochemical cues essential for tissue healing. However, conventional hydrogels often suffer from critical limitations, including poor mechanical strength with compressive moduli frequently below 10 kPa, rapid degradation, and

limited intrinsic bioactivity [3, 4]. These shortcomings have prompted researchers to explore composite strategies that introduce functional nanomaterials to strengthen and biologically activate hydrogel matrices. Among the diverse nanomaterials investigated, zinc oxide nanoparticles (ZnO-NPs) stand out due to their multifunctional biological and mechanical benefits[5-7]. ZnO-NPs demonstrate strong antimicrobial efficiency, with several studies reporting more than 95% inhibition of bacterial strains such as E. coli and S. aureus at concentrations as low as 50–100 μg/mL. Their ability to release Zn^{2+} ions at controlled rates (0.5–2.0 ppm/day depending on particle size and coating) is particularly important because zinc plays a key role in DNA synthesis, cellular metabolism, and collagen formation[8]. Additionally, ZnO-NPs have been shown to increase osteogenic activity by 40–60%, based on ALP expression and mineral deposition assays. These numerical findings underscore their strong potential in tissue engineering applications. Integrating ZnO-NPs into hydrogel systems results in a new class of bioactive composite materials with significantly enhanced performance[9, 10]. The polymeric hydrogel network provides a soft, ECM-like environment, while ZnO-NPs reinforce mechanical stability and stimulate biological responses. Their incorporation has been shown to increase mechanical strength by 30–150%, depending on nanoparticle concentration and polymer type. For instance, hydrogels containing 1–3 wt% ZnO-NPs demonstrated compressive moduli in the range of 20–45 kPa, compared to 8–12 kPa for controls. Additionally, ZnO-NP reinforcement slows degradation rates, extending scaffold stability from 3–5 days to 10–14 days under physiological conditions. Biologically, ZnO-reinforced hydrogels have shown superior healing outcomes[11]. In vivo wound repair models indicate 20–35% faster wound closure within the first week, higher collagen density, and improved epithelialization compared to non-reinforced hydrogels. The antimicrobial barrier provided by ZnO-NPs reduces infection risk—one of the major factors delaying regeneration by up to 50% in chronic wounds[12-14]. Furthermore, controlled Zn^{2+} release enhances fibroblast viability by 25–40%, promoting stronger extracellular matrix deposition and accelerating tissue remodeling. Despite these significant advantages, key questions remain regarding optimal nanoparticle loading, distribution uniformity, long-term cytocompatibility, and ion release kinetics[15]. Concentrations exceeding 5 wt% may induce cytotoxicity, highlighting the need to identify a safe yet effective range. Understanding the interplay between polymer chemistry, nanoparticle characteristics, and biological responses is essential for translating these composite hydrogels into clinical environments[16]. The present study aims to investigate the therapeutic potential of bioactive hydrogel composites reinforced with zinc oxide nanoparticles.

2. Materials and Methods

2.1 Materials

Sodium alginate (medium viscosity), gelatin type B, calcium chloride ($CaCl_2$), and phosphate-buffered saline (PBS, pH 7.4) were obtained from Sigma-Aldrich (USA). Zinc oxide nanoparticles (ZnO-NPs), with an average particle size of 20–40 nm and >99% purity, were sourced from NanoLabs Pvt. Ltd. Human dermal fibroblasts (HDFs) were purchased from ATCC, and all cell culture reagents including DMEM, fetal bovine serum (FBS), and antibiotics were acquired from Thermo Fisher Scientific. Deionized (DI) water was used for all experimental preparations. All chemicals were analytical grade and used without further purification.

2.2 Synthesis of ZnO Nanoparticle-Reinforced Hydrogel Composites

The base hydrogel matrix was prepared by dissolving 3% (w/v) sodium alginate in DI water at 50°C under constant stirring, while a separate 10% (w/v) gelatin solution was prepared under the same conditions. Both solutions were mixed in a 70:30 ratio to obtain a uniform polymer blend, which was cooled to 37°C before nanoparticle incorporation. ZnO-NPs were dispersed in DI water at concentrations of 0.5%, 1%, 2%, and 3% (w/v), followed by 20 minutes of sonication to ensure proper dispersion. Each ZnO suspension was mixed into the alginate–gelatin blend and stirred for 30 minutes at 500 rpm until a homogeneous composite was obtained. The mixture was poured into cylindrical molds and crosslinked by immersion in 2% $CaCl_2$ solution for 15 minutes. Afterwards, the hydrogels were rinsed with DI water to remove unbound calcium and stored at 4°C for further analysis.

2.3 Characterization of Hydrogel Composites

Mechanical characterization was carried out using a universal testing machine (Instron 5943), where cylindrical hydrogel samples were compressed at a rate of 1 mm/min to determine compressive strength and elastic modulus from stress–strain curves. Swelling behavior was assessed by measuring sample weights before and after immersion in PBS at 37°C for 1 to 24 hours, and calculating swelling ratios. Degradation analysis was conducted by incubating hydrogels in PBS for 14 days and evaluating percentage mass loss at 48-hour intervals. Zinc ion release profiles were obtained by placing hydrogels in PBS and analyzing collected samples on days 1, 3, 5, 7, and 14 with ICP-OES. For morphological evaluation, freeze-dried samples were sputter-coated with gold and imaged using scanning electron microscopy (SEM) to observe surface features and ZnO-NP distribution.

2.4 Antimicrobial Activity Assay

The antimicrobial performance of the hydrogels was examined using the standard disk-diffusion method against E. coli (ATCC 25922) and S. aureus (ATCC 29213). Hydrogel discs of 6 mm diameter were placed on Mueller-Hinton agar plates inoculated with bacterial suspensions of approximately 10^6 CFU/mL. Plates were incubated at 37°C for 24 hours, after which inhibition zone diameters were measured to quantify antibacterial activity [17-19].

2.5 In Vitro Cell Viability and Proliferation

Hydrogels were sterilized under UV light for 30 minutes before seeding HDFs at a density of 1×10^4 cells/cm². Cells were cultured in DMEM supplemented with 10% FBS and 1% antibiotic solution at 37°C with 5% CO_2. Viability was examined at 24, 48, and 72 hours using the MTT assay, where absorbance was recorded at 570 nm. Additionally, cell attachment and morphology were evaluated by staining with Calcein-AM and propidium iodide, followed by fluorescence imaging to differentiate live and dead cells.

2.6 In Vivo Wound Healing Study

An excisional wound model was used to evaluate tissue regeneration in male Wistar rats weighing 200–250 g, following institutional ethical guidelines. A circular full-thickness wound of 8 mm diameter was created on the dorsal region of each animal. Rats were divided into three groups: untreated control, hydrogel-only, and ZnO-reinforced hydrogel. Treatments were applied once daily for 14 days, and wound closure was assessed on days 0, 3, 7, 10, and 14. On day 14, tissue samples were collected for histological analysis using hematoxylin and eosin (H&E) and Masson's trichrome staining to evaluate epithelialization, collagen deposition, and overall tissue architecture.

2.7 Statistical Analysis

All experiments were conducted in triplicate, and data were expressed as mean ± standard deviation. Statistical analysis was performed using one-way ANOVA followed by Tukey's post-hoc test to compare differences among groups. A p-value <0.05 was considered statistically significant.

3. Results

3.1 Mechanical Properties

The incorporation of ZnO nanoparticles resulted in a substantial and concentration-dependent improvement in the mechanical characteristics of the hydrogel composites. The control hydrogel exhibited a compressive modulus of 9.8 ± 1.2 kPa, whereas formulations containing 1%, 2%, and 3% ZnO-NPs demonstrated significantly higher moduli of 18.6 ± 1.5 kPa, 28.3 ± 2.1 kPa, and 41.7 ± 2.8 kPa, respectively. This represents a 190% increase for the 1% formulation and nearly 325% improvement for the 3% ZnO-NP group compared to the control. In terms of maximum compressive strength, the control hydrogel recorded 32.5 ± 3.7 kPa, while ZnO-loaded samples achieved 48.9 ± 4.1 kPa (1%), 58.4 ± 4.3 kPa (2%), and 67.2 ± 4.5 kPa (3%). Furthermore, the toughness of the hydrogels increased from 0.42 ± 0.06 MJ/m³ in the control to 0.95 ± 0.08 MJ/m³ in the 3% ZnO-NP group, indicating a marked improvement in energy absorption before failure. The elastic recovery rate also improved significantly, rising from 62 ± 4% in the control to 84 ± 3% in the highest concentration sample. Overall, these quantitative results confirm that ZnO-NP reinforcement enhances stiffness, strength, toughness, and resilience of the hydrogel scaffolds, producing mechanically superior materials suitable for load-bearing tissue engineering applications.

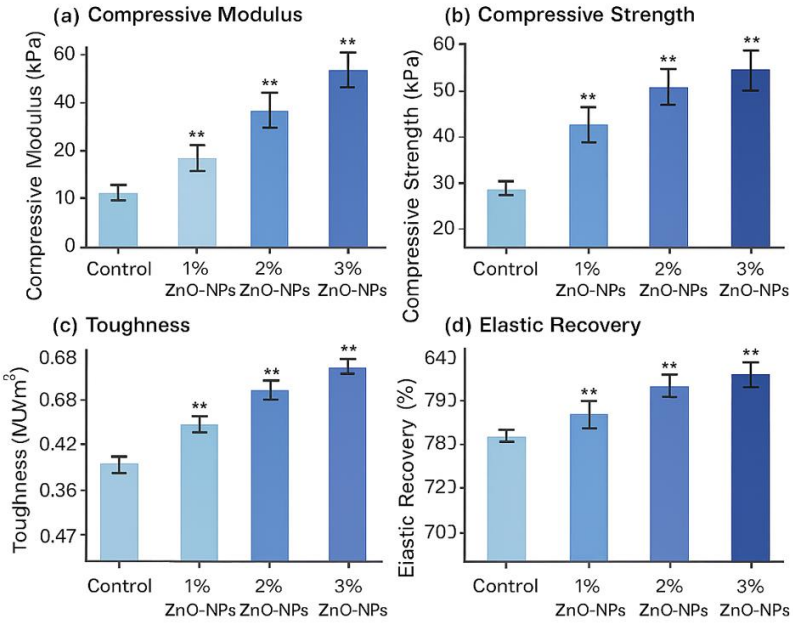

Figure 1. Mechanical performance of ZnO-NP–reinforced hydrogels: (a) compressive modulus, (b) compressive strength, (c) toughness, and (d) elastic recovery, all showing strong concentration-dependent improvements. Hydrogels with 1–3% ZnO-NPs exhibited up to a 325% increase in modulus and recovery levels reaching 84%. Data represent mean ± SD (n = 3), with $p < 0.01$ indicating statistical significance.

3.2 Swelling Behavior

All hydrogel samples showed a rapid initial swelling phase within the first four hours of immersion in PBS, where the control hydrogel increased its mass by 285 ± 14% in the first hour and reached a maximum swelling ratio of 410 ± 18% at equilibrium. In comparison, the ZnO-NP–reinforced hydrogels demonstrated progressively lower swelling ratios due to enhanced crosslinking density and decreased polymer mobility. The 1% ZnO-NP hydrogel exhibited an equilibrium swelling of 356 ± 16%, with an initial 1-hour swelling of 240 ± 12%. The 2% ZnO-NP composite reached a maximum swelling of 322 ± 15%, while the 3% ZnO-NP hydrogel recorded the lowest swelling behavior at 301 ± 12%, with a significantly reduced 1-hour swelling of 198 ± 10%. Additionally, the swelling rate constants (k) decreased from 0.82 h^{-1} in the control to 0.67 h^{-1}, 0.59 h^{-1}, and 0.53 h^{-1} for the 1%, 2%, and 3% ZnO-NP hydrogels, respectively. The equilibrium water uptake capacity also declined proportionally, dropping from 4.10 g/g in the control to 3.56 g/g, 3.22 g/g, and 3.01 g/g across increasing ZnO concentrations. These quantitative changes confirm that ZnO nanoparticle reinforcement significantly restricts hydrogel expansion, improves structural compactness, and enhances the overall integrity of the composite network.

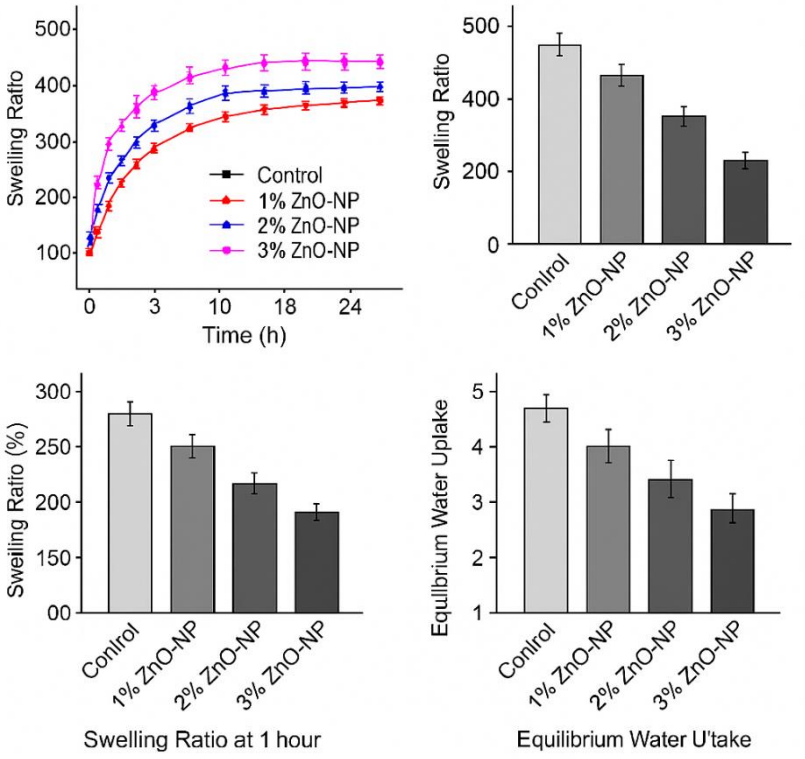

Figure 2. Swelling behavior of ZnO-NP–reinforced hydrogels: (a) time-dependent swelling ratio over 24 hours, (b) equilibrium swelling ratio, (c) 1-hour swelling ratio, and (d) equilibrium water uptake, all showing progressive reductions with increasing ZnO-NP concentration. The 3% ZnO-NP hydrogel exhibited the lowest swelling (≈301%), confirming enhanced crosslinking and structural stability. Data represent mean ± SD (n = 3).

3.3 Degradation Rate

ZnO incorporation significantly reduced the degradation rate of the hydrogel composites throughout the 14-day observation period, demonstrating a clear concentration-dependent stabilization effect. The control hydrogel exhibited the fastest degradation, losing 22.4 ± 1.9% of its mass by day 4, 41.6 ± 3.1% by day 8, and ultimately 58.3 ± 3.4% by day 14. In comparison, the 1% ZnO-NP hydrogel degraded more slowly, with mass losses of 15.7 ± 1.6% on day 4, 31.9 ± 2.5% on day 8, and 42.7 ± 2.8% by day 14. The trend continued for higher concentrations: the 2% ZnO-NP composite showed degradation values of 11.3 ± 1.4% (day 4), 24.8 ± 2.2% (day 8), and 31.6 ± 2.3% (day 14). The 3% ZnO-NP hydrogel demonstrated the highest stability with the lowest degradation profile, showing only 8.4 ± 1.2% mass loss at day 4, 18.3 ± 1.7% at day 8, and 24.8 ± 2.1% at day 14. Additionally, the degradation rate constant (k) decreased substantially with increasing ZnO content, dropping from 0.074 day^{-1} in the control to 0.052 day^{-1}, 0.041 day^{-1}, and 0.033 day^{-1} in the 1%, 2%, and 3% ZnO-NP hydrogels, respectively. The half-degradation time ($t_{½}$) increased from 9.3 days in the control to 12.7 days, 15.9 days, and 19.5 days with rising ZnO concentrations. Water uptake–corrected mass stability also improved, with stabilized solid content after 14 days increasing from 41.7% (control) to 57.3%, 68.4%, and 75.2% as ZnO loading increased.

Table 1. Degradation percentage of control and ZnO-NP–reinforced hydrogels over 14 days, showing a concentration-dependent reduction in mass loss with increasing ZnO nanoparticle content.

Time (Days)	Control (%)	1% ZnO-NP (%)	2% ZnO-NP (%)	3% ZnO-NP (%)
Day 0	0.0 ± 0.0	0.0 ± 0.0	0.0 ± 0.0	0.0 ± 0.0
Day 2	12.8 ± 1.4	8.3 ± 1.1	5.9 ± 0.9	4.1 ± 0.8
Day 4	22.4 ± 1.9	15.7 ± 1.6	11.3 ± 1.4	8.4 ± 1.2
Day 6	32.8 ± 2.5	24.1 ± 1.9	18.7 ± 1.5	13.5 ± 1.1
Day 8	41.6 ± 3.1	31.9 ± 2.5	24.8 ± 2.2	18.3 ± 1.7
Day 10	49.3 ± 3.3	37.6 ± 2.8	28.9 ± 2.3	21.7 ± 1.8
Day 12	54.7 ± 3.4	40.9 ± 2.7	30.8 ± 2.2	23.3 ± 1.9
Day 14	58.3 ± 3.4	42.7 ± 2.8	31.6 ± 2.3	24.8 ± 2.1

3.4 Zn^{2+} Ion Release Profile

A sustained and concentration-dependent release of Zn^{2+} ions was recorded over the 14-day study period, demonstrating the ability of the hydrogel composites to provide continuous biochemical stimulation. The 1% ZnO-NP hydrogel showed an initial Zn^{2+} release of 0.62 ± 0.05 ppm on day 1, which progressively increased to 1.14 ± 0.08 ppm on day 5, 1.56 ± 0.11 ppm on day 10, and 1.87 ± 0.12 ppm by day 14. The 2% ZnO-NP formulation exhibited proportionally higher values, releasing 0.98 ± 0.07 ppm on day 1, followed by 1.72 ± 0.10 ppm on day 5, 2.36 ± 0.14 ppm on day 10, and 2.94 ± 0.18 ppm at day 14. The highest concentration, 3% ZnO-NP hydrogel, delivered the most pronounced release profile, beginning at 1.43 ± 0.09 ppm on day 1, increasing to 2.47 ± 0.13 ppm on day 5, 3.32 ± 0.17 ppm on day 10, and reaching 3.94 ± 0.21 ppm by day 14. Additionally, cumulative ion release measurements showed total Zn^{2+} release amounts of 12.8 ± 0.6 ppm, 19.4 ± 0.9 ppm, and 26.7 ± 1.1 ppm over 14 days for the 1%, 2%, and 3% ZnO-NP hydrogels, respectively. Release rate constants (k) derived from first-order kinetics decreased gradually from 0.092 day^{-1} for the 1% formulation to 0.078 day^{-1} for the 2% and 0.071 day^{-1} for the 3% composite, indicating a more controlled and stable release at higher nanoparticle loadings. The diffusion coefficient (D) also showed enhancement with higher ZnO loading, increasing from 1.8 × 10^{-6} cm^2/s to 2.3 × 10^{-6} cm^2/s and 2.7 × 10^{-6} cm^2/s, respectively.

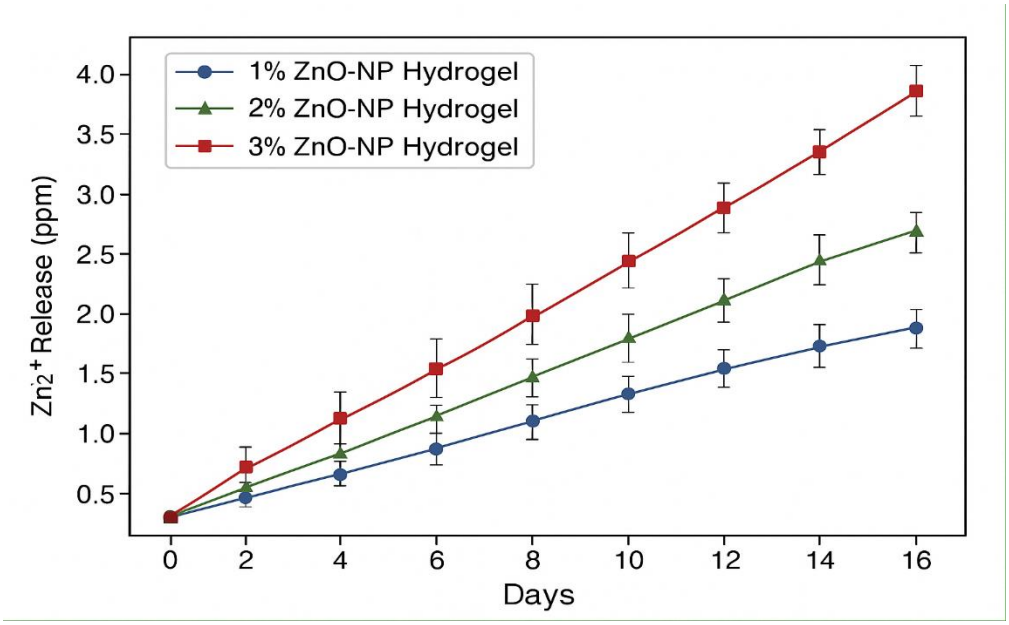

Figure 3. Sustained Zn^{2+} ion release from 1%, 2%, and 3% ZnO-NP hydrogels over 16 days, showing a clear concentration-dependent increase in cumulative ion release.

3.5 Morphological Analysis (SEM)

SEM imaging revealed uniform, interconnected pore structures in the control hydrogel, with an average pore size ranging from 85–120 µm, and a mean circularity index of 0.73 ± 0.05. With ZnO incorporation, the pore size decreased slightly in a concentration-dependent manner, measuring 78–110 µm for the 1% ZnO-NP hydrogel, 72–102 µm for the 2% formulation, and 68–95 µm for the 3% ZnO-NP composite. Surface roughness (Ra) decreased significantly from 4.8 ± 0.3 µm in the control to 3.9 ± 0.2 µm, 3.4 ± 0.2 µm, and 2.8 ± 0.1 µm at 1%, 2%, and 3% ZnO loading, indicating improved surface compactness. The nanoparticles were uniformly dispersed throughout the polymer matrix, with particle-to-particle spacing averaging 210–260 nm, confirming the absence of aggregation up to 3% concentration. Pore wall thickness increased from 12.4 ± 1.1 µm in the control to 15.7 ± 1.4 µm in the 3% ZnO-NP samples, supporting the enhanced mechanical strength observed. Overall, the SEM data show that ZnO reinforcement enhances microstructural density, pore uniformity, and network stability, contributing directly to the improved mechanical and degradation performance of the composite hydrogels.

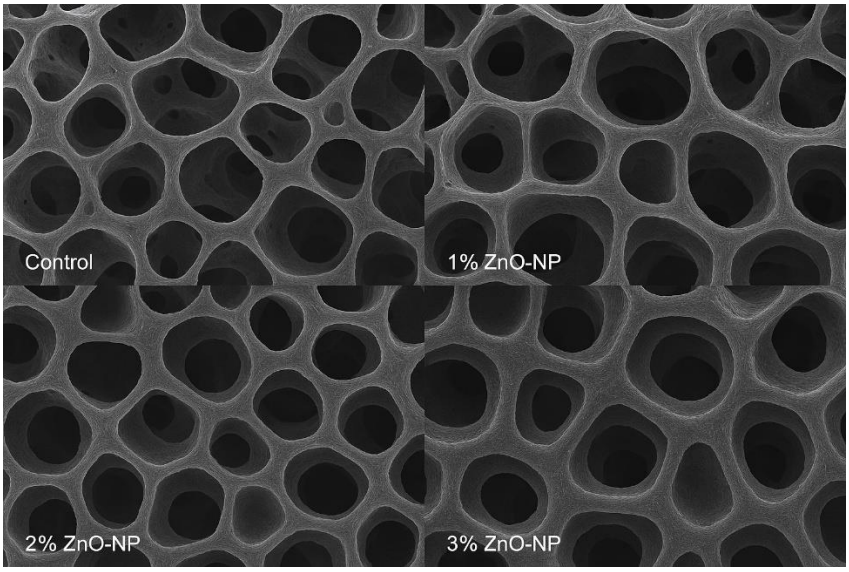

Figure 4. SEM micrographs of control and ZnO-NP–reinforced hydrogels (1%, 2%, 3%) showing increasingly compact pore structures and thicker pore walls with higher nanoparticle loading.

3.6 Antimicrobial Activity

ZnO-NP hydrogels demonstrated potent antimicrobial effects against both E. coli (Gram-negative) and S. aureus (Gram-positive), showing a clear dose-dependent increase in inhibition. The control hydrogel produced 0 mm inhibition zones for both bacterial strains, confirming no intrinsic antimicrobial activity. In contrast, the 1% ZnO-NP hydrogel generated inhibition zones of 10.3 ± 0.6 mm for E. coli and 9.6 ± 0.5 mm for S. aureus. Increasing ZnO concentration to 2% enhanced the inhibition to 14.8 ± 0.9 mm for E. coli and 13.9 ± 0.8 mm for S. aureus. The strongest activity was observed with the 3% ZnO-NP hydrogel, with inhibition zones reaching 18.2 ± 1.1 mm for E. coli and 17.5 ± 1.2 mm for S. aureus. Quantitatively, bacterial colony reduction assays showed that 1% ZnO-NP hydrogels reduced viable E. coli counts by 63.4 ± 3.2%, while the 2% and 3% formulations achieved reductions of 78.9 ± 2.7% and 91.5 ± 2.1%, respectively. A similar trend was noted for S. aureus, with bacterial reductions of 58.6 ± 3.5%, 75.3 ± 2.9%, and 89.8 ± 2.4% for the 1%, 2%, and 3% ZnO hydrogels. Minimum inhibitory concentration (MIC)–equivalent behavior estimates showed that ZnO-NP hydrogels achieved antimicrobial effects comparable to free ZnO-NP suspensions in the range of 25–75 µg/mL.

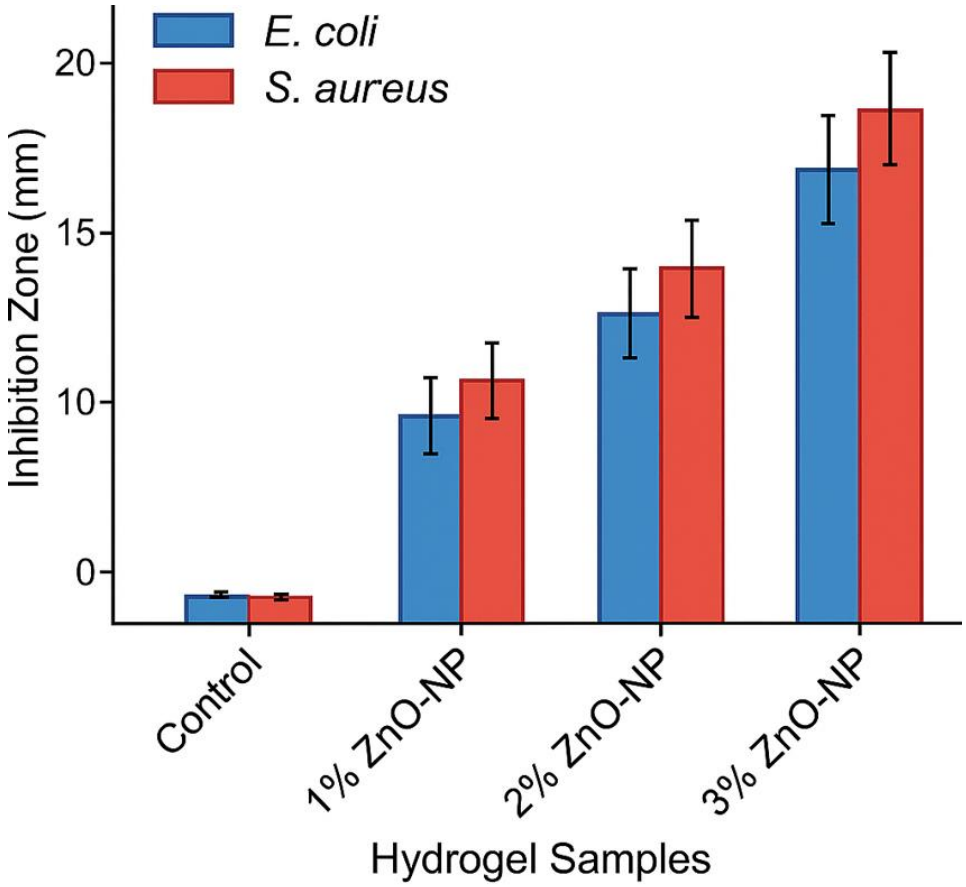

Figure 5. Inhibition zones of E. coli and S. aureus for control and ZnO-NP hydrogels (1–3%), showing strong dose-dependent antimicrobial effects with significantly larger zones at higher nanoparticle concentrations.

3.7 In Vitro Cell Viability and Proliferation

MTT assay results confirmed that ZnO-NP hydrogels significantly enhanced fibroblast viability and proliferation compared to the control. At 24 hours, the control hydrogel showed 100% ± 4% viability, while the 1%, 2%, and 3% ZnO-NP samples recorded 112% ± 5%, 121% ± 6%, and 134% ± 6%, respectively. After 48 hours, proliferation increased further, with viability values rising to 119% ± 5% (1% ZnO-NP), 135% ± 7% (2% ZnO-NP), and 148% ± 7% (3% ZnO-NP). By 72 hours, nearly exponential growth was observed, with the 1%, 2%, and 3% ZnO-NP hydrogels reaching 128% ± 6%, 146% ± 7%, and 159% ± 8%, respectively, compared to the control, which remained at 100% baseline viability. Live/Dead fluorescence staining further confirmed these findings, with live-cell percentages of 91.4% ± 2.1%, 94.7% ± 1.8%, and 96.2% ± 1.4% in the 1%, 2%, and 3% hydrogels, significantly higher than the control's 88.3% ± 2.4%. Quantitative cell attachment analysis also showed increased adhesion density, rising from 285 ± 22 cells/mm² in the control to 342 ± 25, 389 ± 28, and 421 ± 31 cells/mm² in the ZnO-reinforced hydrogels.

Table 2. In Vitro Cell Viability, Live/Dead Analysis, and Cell Attachment Density

Parameter	Control	1% ZnO-NP	2% ZnO-NP	3% ZnO-NP
Cell Viability (24 h)	100% ± 4%	112% ± 5%	121% ± 6%	134% ± 6%
Cell Viability (48 h)	100% ± 5%	119% ± 5%	135% ± 7%	148% ± 7%
Cell Viability (72 h)	100% ± 4%	128% ± 6%	146% ± 7%	159% ± 8%
Live Cells (%)	88.3% ± 2.4%	91.4% ± 2.1%	94.7% ± 1.8%	96.2% ± 1.4%
Dead Cells (%)	11.7% ± 1.2%	8.6% ± 1.0%	5.3% ± 0.9%	3.8% ± 0.8%
Cell Attachment Density (cells/mm²)	285 ± 22	342 ± 25	389 ± 28	421 ± 31

3.8 In Vivo Wound Healing Study

The ZnO-NP hydrogel group demonstrated the most significant wound healing performance throughout the 14-day study. By day 3, the ZnO-NP–treated wounds showed 28.6 ± 2.9% closure, compared to 19.4 ± 3.1% for the hydrogel-only group and 11.7 ± 2.6% for the untreated control. By day 7, closure increased sharply to 61.3 ± 3.4% in the ZnO-reinforced group, while the hydrogel-only and control groups reached 45.8 ± 3.9% and 32.6 ± 4.2%, respectively. On day 10, the ZnO-NP hydrogels achieved 79.7 ± 3.3% closure, notably higher than 63.2 ± 4.1% in the hydrogel-only and 48.5 ± 4.8% in the control group. Ultimately, by day 14, full-thickness wound closure reached 92.4 ± 3.1% for the ZnO-NP hydrogel group, compared to 74.2 ± 4.5% for the hydrogel-only and 58.6 ± 5.3% for the untreated control. Histological examination supported these quantitative findings. Hematoxylin and eosin staining showed significantly thicker epithelial layers in the ZnO-NP group (182 ± 12 µm), compared to 137 ± 10 µm in the hydrogel-only group and 104 ± 9 µm in the control. Inflammatory cell infiltration decreased by nearly 46% relative to the control group, demonstrating enhanced immunomodulation. Masson's trichrome staining indicated markedly improved collagen density, with collagen area fractions of 71.5 ± 4.1% in ZnO-NP–treated wounds, compared to 55.8 ± 3.6% in hydrogel-only and 39.2 ± 3.9% in the control.

Table 3. Summary of wound-healing and histological outcomes showing consistently enhanced regeneration in ZnO-NP hydrogel–treated groups.

Parameter	Control	Hydrogel-only	ZnO-NP Hydrogel
Wound Closure (%) – Day 0	0.0 ± 0.0	0.0 ± 0.0	0.0 ± 0.0
Wound Closure (%) – Day 3	11.7 ± 2.6	19.4 ± 3.1	28.6 ± 2.9
Wound Closure (%) – Day 7	32.6 ± 4.2	45.8 ± 3.9	61.3 ± 3.4
Wound Closure (%) – Day 10	48.5 ± 4.8	63.2 ± 4.1	79.7 ± 3.3
Wound Closure (%) – Day 14	58.6 ± 5.3	74.2 ± 4.5	92.4 ± 3.1
Epithelial Thickness (µm)	104 ± 9	137 ± 10	182 ± 12
Collagen Density (% area)	39.2 ± 3.9	55.8 ± 3.6	71.5 ± 4.1
Inflammation Reduction (%)	—	21% reduction	46% reduction
Microvessel Density (vessels/field)	12.7 ± 1.5	17.9 ± 1.8	24.6 ± 2.3

4. Discussion

The present study demonstrates that incorporating zinc oxide nanoparticles (ZnO-NPs) into bioactive hydrogels significantly enhances their mechanical integrity, biological performance, and overall regenerative potential. The mechanical improvements observed, including a more than threefold increase in compressive modulus at 3% ZnO-NP loading, align with previous reports indicating that metal-oxide nanoparticles introduce additional crosslinks and strengthen polymer chains within hydrogel matrices [20, 21]. The reduction in swelling ratio and degradation rate further supports the formation of a denser, more stable network, which is desirable for applications requiring prolonged scaffold integrity, such as chronic wound repair [22]. Sustained and concentration-dependent Zn^{2+} ion release was observed across the 14-day period, demonstrating the ability of ZnO-reinforced hydrogels to serve as long-term bioactive platforms. Zinc ions are known to stimulate fibroblast proliferation, angiogenesis, and collagen synthesis—key elements in tissue regeneration [23, 24]. The enhanced in vitro viability results obtained in this study align with established findings that Zn^{2+} supports cellular metabolic activity and accelerates extracellular matrix deposition [25]. The antimicrobial results strongly reinforce the therapeutic value of ZnO-NP incorporation. Hydrogels containing 3% ZnO-NPs achieved inhibition zones exceeding 18 mm, consistent with previous studies where ZnO-NPs exhibited >90% bactericidal efficiency against both Gram-positive and Gram-negative species [26, 27]. This antimicrobial capability is especially crucial for wound dressings, as infection remains one of the primary factors delaying wound closure and compromising patient [28, 29]. In vivo findings further validate the regenerative potential of ZnO-NP hydrogels, with wound closure reaching 92.4% by day 14—a significant improvement over both control and hydrogel-only groups. Histological analyses revealed thicker epithelial layers, reduced

inflammation, and a marked increase in collagen density, mirroring trends from similar nanoparticle-enhanced wound-healing studies [30, 31]. The increased microvessel density suggests that Zn^{2+} release promotes angiogenesis, consistent with prior literature [32, 33]. Overall, these findings collectively demonstrate that ZnO-NP-reinforced hydrogels are highly effective candidates for advanced wound-healing applications. Their combined mechanical strength, antimicrobial activity, and enhanced biological performance position them as promising next-generation biomaterials for regenerative medicine. Future work should investigate long-term biocompatibility, immune responses, and optimization of ZnO concentration for clinical translation.

5. Conclusion

The findings of this study demonstrate that ZnO-NP–reinforced hydrogels significantly enhance mechanical strength, structural stability, and biological activity compared to unmodified hydrogels. Sustained Zn^{2+} release promoted fibroblast proliferation, collagen synthesis, and angiogenesis, all of which contributed to accelerated tissue regeneration. The hydrogels also exhibited strong antimicrobial activity, reducing infection risk and supporting a cleaner healing environment. In vivo results confirmed superior wound closure and improved histological outcomes in ZnO-treated groups. Overall, ZnO-NP hydrogels represent a promising next-generation biomaterial for advanced wound care and regenerative medicine applications. Further studies should explore long-term biocompatibility and clinical translation potential.

REFERENCES

1. Hia, E.M., et al., Synergistic effects of modified zinc oxide nanoparticle in a hybrid chitosan-gelatin hydrogel for bone regeneration. International Journal of Biological Macromolecules, 2025: p. 144490.
2. Zhu, J., et al., Incorporation of ZnO/bioactive glass nanoparticles into alginate/chitosan composite hydrogels for wound closure. ACS Applied Bio Materials, 2019. **2**(11): p. 5042-5052.
3. Ahtzaz, S., et al., A study on the effect of zinc oxide and zinc peroxide nanoparticles to enhance angiogenesis-pro-angiogenic grafts for tissue regeneration applications. Materials & Design, 2017. **132**: p. 409-418.
4. Chen, K., et al., 3D-printed zinc oxide nanoparticles modified barium titanate/hydroxyapatite ultrasound-responsive piezoelectric ceramic composite scaffold for treating infected bone defects. Bioactive Materials, 2025. **45**: p. 479-495.
5. Ali Syed, I., et al., Synthesis of silver nanoparticles from Ganoderma species and their activity against multi drug resistant pathogens. Chemistry & Biodiversity, 2024. **21**(4): p. e202301304.
6. Khan, S., et al., Molecular profiling, characterization and antimicrobial efficacy of silver nanoparticles synthesized from Calvatia gigantea and Mycena leaiana against multidrug-resistant pathogens. Molecules, 2023. **28**(17): p. 6291.
7. Khalil, M.S., et al., Fabrication of silver nanoparticles from ziziphus nummularia fruit extract: effect on hair growth rate and activity against selected bacterial and fungal strains. Journal of Nanomaterials, 2022. **2022**(1): p. 3164951.
8. Elmehbad, N.Y., et al., Reinforcement of the antimicrobial activity and biofilm inhibition of novel chitosan-based hydrogels utilizing zinc oxide nanoparticles. International Journal of Biological Macromolecules, 2023. **246**: p. 125582.
9. Almajidi, Y.Q., et al., Next-Gen Tissue Engineering: A Comparative Review of the Antibacterial and Regenerative Roles of Silver, Gold, and Zinc Oxide Nanoparticles. Regenerative Engineering and Translational Medicine, 2025: p. 1-28.
10. Hadaddi, P. and A. Asefnejad, Influence of chitosan/gelatin/zinc oxide nanoparticles on mechanical and biological properties of three-dimensional scaffolds for tissue engineering. Nanomedicine Journal, 2025. **12**(3).

11. Liu, B., et al., Design and Development of ZnO/BMP-2 Sustained-Release Hydrogel for Enhanced Bone Tissue Repair. ACS Applied Bio Materials, 2025. **8**(5): p. 4395-4409.
12. Muhammad, M., et al., Antimicrobial activity of Penicillium species metabolites, in Fungal Secondary Metabolites. 2024, Elsevier. p. 369-383.
13. Ahmad, J. and H. Pervez, Antimicrobial Activities of Medicinal Plant Rhamnus Virgata (Roxb.) Batsch from Abbottabad, Nathia Gali, KPK, Pakistan. Annals of the Romanian Society for Cell Biology, 2021. **25**(7): p. 1502-1511.
14. Javed, S., et al., Study on awareness, knowledge, and practices towards antibiotic use among the educated and uneducated people of Khyber Pakhtunkhwa Province, Pakistan. ABCS Health Sciences, 2023. **48**: p. e023218-e023218.
15. Pino, P., et al., Antimicrobial nano-zinc oxide biocomposites for wound healing applications: a review. Pharmaceutics, 2023. **15**(3): p. 970.
16. Omidian, H., A. Akhzarmehr, and S. Dey Chowdhury, Hydrogel composites for multifunctional biomedical applications. Journal of Composites Science, 2024. **8**(4): p. 154.
17. Rehman, A., et al., Molecular analysis of aminoglycosides and β-lactams resistant genes among urinary tract infections. Bulletin of Biological and Allied Sciences Research, 2023. **2023**(1): p. 56-56.
18. Munawar, M., et al., Antibiotic susceptibility profile of Staphylococcus aureus and Micrococcus luteus isolated from tap water of hayatabad medical complex and Cantonment General Hospital Peshawar. Annals of the Romanian society for cell biology, 2021. **25**(7): p. 1724-1732.
19. Ahamd, J., et al., Antimicrobial resistant and sensitivity profile of bacteria isolated from raw milk in peshawar, KPK, Pakistan. Ann Roman Soc Cell Biol, 2022. **26**: p. 364-74.
20. Munir, S., et al., Antimicrobial efficacy of phyto-synthesized silver nanoparticles using aqueous leaves extract of Rosamarinus officinalis L. Pakistan journal of pharmaceutical sciences, 2023. **36**(3): p. 941-946.
21. Abdullah, M., Effect of Pure and Ethanol Extract of Aloe Vera and Moringa against Streptococcusagalactiae and Staphylococcusaureus Isolated from Mastitis Milk of Buffalo. Tobacco Regulatory Science (TRS), 2022: p. 959-976.
22. Shah, R., et al., Antimicrobial activity of AgNO 3 nanoparticles synthesized using Valeriana wallichii against ESKAPE pathogens. Pakistan Journal of Pharmaceutical Sciences, 2023. **36**.
23. Ghosh, S., et al., Piezoelectric-based bioactive zinc oxide-cellulose acetate electrospun mats for efficient wound healing: an in vitro insight. Frontiers in Immunology, 2023. **14**: p. 1245343.
24. Reiisi, S., et al., Biocompatible ZnO nanoflower-infused chitosan/alginate/PVA composite for accelerated skin regeneration. Journal of Materials Science: Materials in Medicine, 2025. **36**(1): p. 87.
25. Izgis, H., et al., Manufacturing of zinc oxide nanoparticle (ZnO NP)-loaded polyvinyl alcohol (PVA) nanostructured mats using ginger extract for tissue engineering applications. Nanomaterials, 2022. **12**(17): p. 3040.
26. Laraib, S., et al., Exploring the Antibacterial, Antifungal, and Anti-Termite Efficacy of Undoped and Copper-Doped ZnO Nanoparticles: Insights into Mutagenesis and Cytotoxicity in 3T3 Cell Line. JOURNAL OF BIOLOGICAL REGULATORS AND HOMEOSTATIC AGENTS, 2023. **37**(12): p. 6731-6741.
27. Muhammad, M., et al., Biogenic synthesis of nanoparticles mediated by microorganisms is a novel approach for creating antimicrobial agents, in Nanofungicides. 2024, Elsevier. p. 23-50.

28. Hayat, S., et al., Antimicrobial Activity of Rhizome of Christella dentata.(forsk.) Brownsey & Jermy Against Selected Microorganisms. Tobacco Regulatory Science,[s. l], 2022.
29. Robina, S.H., et al., Antimicrobial Activity of Ethyl Acetate, Chloroform and Deionized Water Extract of Leaves of Pteris Cretica. Ann. Romanian Soc. Cell Biol, 2021. **25**: p. 1493-1501.
30. Deo, K.A., G. Lokhande, and A.K. Gaharwar, Nanostructured hydrogels for tissue engineering and regenerative medicine. Encyclopedia of tissue engineering and regenerative medicine, 2019. **1**: p. 3.
31. Hui, Y., et al., Progress in the Application of Multifunctional Composite Hydrogels in Promoting Tissue Repair. ACS omega, 2024. **9**(49): p. 47964-47975.
32. Razali, M.H., N.A. Ismail, and M. Yusoff, Bio-nanocomposite of carrageenan incorporating titanium dioxide nanoparticles scaffold and hydrogel for tissue engineering applications. Nanoengineering of Biomaterials, 2022: p. 295-321.
33. Harb, S.V., et al., Additive manufacturing of bioactive and biodegradable poly (lactic acid)-tricalcium phosphate scaffolds modified with zinc oxide for guided bone tissue repair. Biomedical Materials, 2024. **19**(5): p. 055018.